Article

Not peer-reviewed version

Second-Order Multiscale Analysis and Algorithms for Composite Mindlin Plate and Timoshenko Beam

Mengyu Zhang , Qiang Ma * , Qinglin Tang

Posted Date: 10 October 2025

doi: 10.20944/preprints202510.0731.v1

Keywords: multiscale characterization; second-order two-scale (SOTS) analysis; finite element method; structural application; Mindlin plate; Timoshenko beam

Article

Second-Order Multiscale Analysis and Algorithms for Composite Mindlin Plate and Timoshenko Beam

Mengyu Zhang, Qiang Ma * and Qinglin Tang

School of Mathematics, Sichuan University, Chengdu 610065, China
* Correspondence: maqiang809@scu.edu.cn

Abstract

This work presents a comprehensive framework for the multiscale characterization of advanced composite structures, focusing on Mindlin plates and Timoshenko beams with periodic microstructures. Using a second-order two-scale (SOTS) method, we uniformly derive asymptotic expansions for deflection and rotation to formulate effective homogenized models. The developed finite element procedures combine techniques to overcome shear locking, enabling efficient and accurate structural application. Numerical simulations verified the convergence of the model and demonstrated its superiority in capturing the rapid oscillation of local stress distribution, an important aspect for the design of reliable composites. By varying the thickness parameter, our model is shown to connect thin and thick theories for composite beam and plate problems. It thus provides a practical tool for the design and analysis of tailored composite structures, contributing to the development of innovative materials.

Keywords: multiscale characterization; second-order two-scale (SOTS) analysis; finite element method; structural application; Mindlin plate; Timoshenko beam

1. Introduction

The transition between precise material characterization and reliable structural application is a core challenge in the development of advanced composite materials. To achieve this goal, we need to establish a unified model that can accurately describe the complex mechanical behavior of composite materials under different structural forms. In previous works, the composite Kirchhoff plate and Euler beam theories have been widely applied in the thin structures [1,2]. However, due to the assumption that cross-section after deformation is perpendicular to the neutral axis and the lateral shear effect is ignored, the deviation is relatively large when simulating moderate thick composite materials. In this case, it is necessary to consider the composite Mindlin plate [3] and Timoshenko beam models, which can recover the Kirchhoff plate and Euler beam models as the thickness decreases. It has provided convenience for the efficient characterization and simulation of the effectiveness of modern composite materials.

Modern composite materials, composed of two or more different materials, such as ultra-high temperature ceramic composite plate reinforced with superalloys, carbon fiber reinforced epoxy resin composite plate [4,5], are widely used in aerospace, automotive and other high-performance engineering fields. These materials are valued for their outstanding rigidity and superior corrosion resistance, demonstrating remarkable adaptability to specialized application requirements. From a mathematical point of view, solving these equations requires dealing with rapidly varying coefficients. Due to the large scale of calculations, the conventional method incurs significant computational costs. Traditional formulations of plate and beam theory often fall short in capturing the complex behavior of structures with multiple length scales. A practical method proposed to simplify these calculations is the homogenization method [6]. By applying multi-scale expansion, homogenized solutions and cell functions can be obtained to describe both macroscopic and microscopic properties.

 doi:10.20944/preprints202510.0731.v1

This method improves the computational efficiency by homogenizing the microstructure features into effective macroscopic parameters, avoiding the expensive discretization at the microscale. Furthermore, the oscillating behavior of solutions can be effectively corrected. Based on the establishment of mathematical theories about the homogenization method [7–9], the multi-scale finite element method (MsFEM) [10], the heterogeneous multi-scale method (HMM) [11,12], and the variational multi-scale method (VMM) have been proposed and developed. Noticing that only first-order asymptotic analysis was established, Cui and Cao considered second-order asymptotic analysis [13]. Applying this method to simulate the deformation of composite materials is more accurate, and corresponding finite element algorithms have been established [14–16]. This SOTS asymptotic analysis is now applied to a variety of problems, such as thermoelasticity [17–19], elasticity problems [20,21], and so on.

However, significant technical difficulties arise in directly applying this asymptotic expansion to the classical theories of thin structures, namely the Kirchhoff plate and Euler beam problems. In the process of asymptotic expansion and analysis, these problems are described by fourth-order partial differential equations. After conducting an asymptotic analysis of models, it has been demonstrated that three-dimensional composite plate can be simplified to two-dimensional uniform Kirchhoff plate as the thickness h and ε approach zero [22]. Lewiński and Józef used the homogenization method and two-scale expansion method to solve the composite Mindlin plate problem in two dimensions [23]. Zhu and Cui provided a new Second-Order Two-Scale(SOTS) method for the Mindlin plate theory, and the laminated homogenization plate was analyzed [24]. Wang and Cui considered the bending behaviors of composite plate with 3-D periodic configuration and established a SOTS method, proving the approximation property of the solution by energy norm estimation [25]. Huang et al. established a two-scale asymptotic homogenization method for periodic composite Kirchhoff plate and Euler beam [26,27]. Numerical comparisons demonstrated that the current method is both physically acceptable and highly accurate.

As is known that directly establishing the SOTS asymptotic model for the fourth-order Kirchhoff plate and Euler beam directly is not easy, so it is reasonable to alternatively perform this high-order expansion on the second-order equations for Mindlin plate and Timoshenko beam first, and then proceed to consider approximating the corresponding composite Kirchhoff plate and Euler beam by letting the thickness h approach zero. We believe that this two-step strategy can not only obtain the asymptotic behavior of the Mindlin plate and Timoshenko beam, but also capture the local variations of the corresponding Kirchhoff plate and Euler beam. This is the principal idea and the main interest of our work, which are not seen elsewhere to the best of our knowledge. It should also be noted that when h is very small, the zero shear strain constraint leads to the shear locking [28–30], and we will discuss how to avoid this phenomenon in the asymptotic computing.

For these purposes mentioned above, the paper is structured as follows: The governing equations for the composite Mindlin plate and Timoshenko beam are presented in Section 2, and the corresponding SOTS asymptotic expansions are derived in Section 3. The finite element algorithm and symbol definitions for the second-order asymptotic plate and beam models are presented in Section 4. Several numerical examples of the SOTS asymptotic expansions for the Mindlin plate and the Timoshenko beam are given. The approaching behavior for the thick-thin theory of the plate and beam for the stationary problem are shown in Section 5. The conclusion remarks are given in Section 6. For simplicity, the Einstein summation convention is used, where the repeated subscript implies summation.

2. Governing Equations

The configuration of the composite plate with thickness h is typically shown in Figure 1(a). Different constituent materials are periodically distributed in the x_1 and x_2 directions and are homogeneous in the thickness direction. The normalized periodic cell is depicted in Figure 1(b).

Define the two-dimensional middle plane as Ω and the unit cell as Y. With the micro and macro coordinates being $\mathbf{x} = [x_1, x_2] \in \Omega$ and $\mathbf{y} = [y_1, y_2] \in Y$, respectively, a small parameter ε is defined to relate these variables as

$$\mathbf{y} = \frac{\mathbf{x}}{\varepsilon} - \left\lfloor \frac{\mathbf{x}}{\varepsilon} \right\rfloor, \tag{1}$$

where $\lfloor \cdot \rfloor$ is floor operator.

The governing equations for the composite Mindlin plate can be formulated as

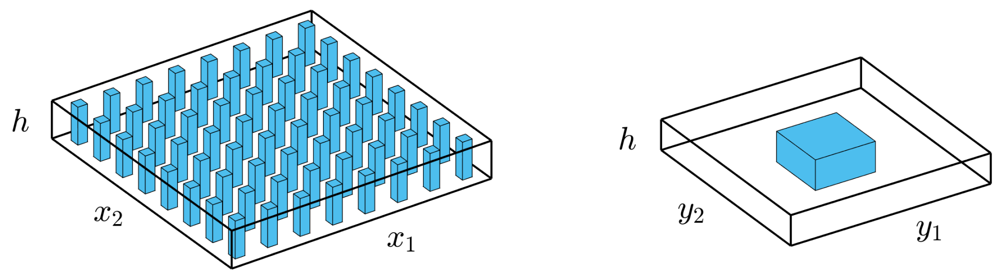

(a) (b)

Figure 1. Composite structures of the plate. **(a)** Composite plate $\Omega \times [-\frac{h}{2}, \frac{h}{2}]$; **(b)** Periodic cell $Y \times [-\frac{h}{2}, \frac{h}{2}]$.

$$\begin{cases} -\dfrac{\partial V_1^\varepsilon}{\partial x_1} - \dfrac{\partial V_2^\varepsilon}{\partial x_2} = q_{\mathrm{M}}, \\ \dfrac{\partial M_1^\varepsilon}{\partial x_1} + \dfrac{\partial M_{12}^\varepsilon}{\partial x_2} - V_1^\varepsilon = 0, \\ \dfrac{\partial M_{12}^\varepsilon}{\partial x_1} + \dfrac{\partial M_2^\varepsilon}{\partial x_2} - V_2^\varepsilon = 0, \end{cases} \tag{2}$$

where V_1^ε and V_2^ε are the shear stresses, M_1^ε and M_2^ε are the bending moments, M_{12}^ε is the torsional moment, and q_{M} represents the external load on the plate.

The shear stress V_1^ε and V_2^ε can be expressed by

$$\begin{bmatrix} V_1^\varepsilon \\ V_2^\varepsilon \end{bmatrix} = \frac{E^\varepsilon k_s h}{2(1+\nu^\varepsilon)} \begin{bmatrix} \dfrac{\partial w^\varepsilon}{\partial x_1} - \beta_1^\varepsilon \\ \dfrac{\partial w^\varepsilon}{\partial x_2} - \beta_2^\varepsilon \end{bmatrix}, \tag{3}$$

where w^ε is the deflection, β_1^ε and β_2^ε are the rotations of the cross section, E^ε is the Young's modulus, k_s is the shear correction factor, and ν^ε is the Poisson's ratio. E^ε and ν^ε are periodic due to the configuration and can be expressed as

$$E^\varepsilon(\mathbf{x}) = E(\frac{\mathbf{x}}{\varepsilon}) = E(\mathbf{y}), \quad \nu^\varepsilon(\mathbf{x}) = \nu(\frac{\mathbf{x}}{\varepsilon}) = \nu(\mathbf{y}), \tag{4}$$

where $E(\mathbf{y})$ and $\nu(\mathbf{y})$ are periodic functions defined in Y. The constitutive relation between bending moment and curvature is given by

$$\begin{bmatrix} M_1^\varepsilon \\ M_2^\varepsilon \\ M_{12}^\varepsilon \end{bmatrix} = \frac{E^\varepsilon h^3}{12(1-(\nu^\varepsilon)^2)} \begin{bmatrix} 1 & \nu^\varepsilon & 0 \\ \nu^\varepsilon & 1 & 0 \\ 0 & 0 & \dfrac{1-\nu^\varepsilon}{2} \end{bmatrix} \begin{bmatrix} -\dfrac{\partial \beta_1^\varepsilon}{\partial x_1} \\ -\dfrac{\partial \beta_2^\varepsilon}{\partial x_2} \\ -\dfrac{\partial \beta_1^\varepsilon}{\partial x_2} - \dfrac{\partial \beta_2^\varepsilon}{\partial x_1} \end{bmatrix}. \tag{5}$$

For simplicity, clamped boundary conditions are imposed on $\partial\Omega$ and the Mindlin plate problem is given as

$$\begin{cases} -\dfrac{\partial}{\partial x_i}\left(k_s G^\varepsilon h\left(\dfrac{\partial w^\varepsilon}{\partial x_i} - \beta_i^\varepsilon\right)\right) = q_{\mathrm{M}} & \text{in } \Omega, \\ -\dfrac{\partial}{\partial x_j}\left(C_{ijkl}^\varepsilon \dfrac{\partial \beta_k^\varepsilon}{\partial x_l}\right) - k_s G^\varepsilon h\left(\dfrac{\partial w^\varepsilon}{\partial x_i} - \beta_i^\varepsilon\right) = 0 & \text{in } \Omega, \\ w^\varepsilon = 0 & \text{on } \partial\Omega, \\ \beta_i^\varepsilon = 0 & \text{on } \partial\Omega, \end{cases} \tag{6}$$

where C_{ijkl}^ε is defined by

$$C_{ijkl}^\varepsilon = \frac{E^\varepsilon h^3 \nu^\varepsilon}{12(1-(\nu^\varepsilon)^2)}\delta_{ij}\delta_{kl} + \frac{E^\varepsilon h^3}{24(1+\nu^\varepsilon)}\left(\delta_{ik}\delta_{jl} + \delta_{il}\delta_{jk}\right), \tag{7}$$

and G^ε is the shear modulus, related to E^ε and ν^ε through $G^\varepsilon = \frac{E^\varepsilon}{2(1+\nu^\varepsilon)}$.

The Timoshenko beam problem is equivalent to the dimensional reduction of the plate problem (6). Therefore, the composite Timoshenko beam problem takes the following form:

$$\begin{cases} -\dfrac{d}{dx_1}\left(k_s G^\varepsilon A\left(\dfrac{dw^\varepsilon}{dx_1} - \beta^\varepsilon\right)\right) = q_{\mathrm{T}} & \text{in } \Omega, \\ -\dfrac{d}{dx_1}\left(E^\varepsilon I \dfrac{d\beta^\varepsilon}{dx_1}\right) - k_s G^\varepsilon A\left(\dfrac{dw^\varepsilon}{dx_1} - \beta^\varepsilon\right) = 0 & \text{in } \Omega, \\ w^\varepsilon = 0 & \text{on } \partial\Omega, \\ \beta^\varepsilon = 0 & \text{on } \partial\Omega, \end{cases} \tag{8}$$

where w^ε is the one-dimensional deflection, β^ε is the rotation, A is the sectional area, given by $A = b \times h$ with b being the width, and q_{T} is the external load on the beam.

3. The SOTS Asymptotic Analysis

First, we perform the SOTS asymptotic analysis for the composite Mindlin plate problems (6). Following the standard procedure, the deflection w^ε, rotation β_i^ε can be expanded as

$$\begin{aligned} w^\varepsilon(\mathbf{x}) &= w_0(\mathbf{x}) + \varepsilon w_1(\mathbf{x},\mathbf{y}) + \varepsilon^2 w_2(\mathbf{x},\mathbf{y}) + O(\varepsilon^3), \\ \beta_i^\varepsilon(\mathbf{x}) &= \beta_i^0(\mathbf{x}) + \varepsilon \beta_i^1(\mathbf{x},\mathbf{y}) + \varepsilon^2 \beta_i^2(\mathbf{x},\mathbf{y}) + O(\varepsilon^3), i = 1,2, \end{aligned} \tag{9}$$

with the homogenized solutions $w_0(\mathbf{x})$, $\beta_i^0(\mathbf{x})$, appended by the first-order correctors $w_1(\mathbf{x},\mathbf{y})$, $\beta_i^1(\mathbf{x},\mathbf{y})$ and the second-order terms $w_2(\mathbf{x},\mathbf{y})$, $\beta_i^2(\mathbf{x},\mathbf{y})$. Transforming the partial derivatives as

$$\frac{\partial}{\partial x_i} \to \frac{\partial}{\partial x_i} + \frac{1}{\varepsilon}\frac{\partial}{\partial y_i}, \tag{10}$$

substituting Eqs. (9) into governing equations (6), and equating the power coefficients of ε, the equations for the first three expansion terms are obtained as follows:

$$O\left(\varepsilon^{-1}\right):\begin{cases} -\dfrac{\partial}{\partial y_i}\left(k_s Gh\dfrac{\partial w_1}{\partial y_i}\right)-\dfrac{\partial}{\partial y_i}\left(k_s Gh\left(\dfrac{\partial w_0}{\partial x_i}-\beta_i^0\right)\right)=0,\\ -\dfrac{\partial}{\partial y_j}\left(C_{ijkl}\dfrac{\partial \beta_k^1}{\partial y_l}\right)-\dfrac{\partial}{\partial y_j}\left(C_{ijkl}\dfrac{\partial \beta_k^0}{\partial x_l}\right)=0,\end{cases} \tag{11}$$

$$O\left(\varepsilon^{0}\right):\begin{cases} -\dfrac{\partial}{\partial x_i}\left(k_s Gh\left(\dfrac{\partial w_1}{\partial y_i}+\dfrac{\partial w_0}{\partial x_i}-\beta_i^0\right)\right)+\dfrac{\partial}{\partial y_i}\left(k_s Gh\beta_i^1\right)\\ \qquad -\dfrac{\partial}{\partial y_i}\left(k_s Gh\dfrac{\partial w_2}{\partial y_i}\right)-\dfrac{\partial}{\partial y_i}\left(k_s Gh\dfrac{\partial w_1}{\partial x_i}\right)=q_{\mathrm{M}},\\ -\dfrac{\partial}{\partial y_j}\left(C_{ijkl}\dfrac{\partial \beta_k^2}{\partial y_l}\right)-\dfrac{\partial}{\partial x_j}\left(C_{ijkl}\dfrac{\partial \beta_k^1}{\partial y_l}\right)-\dfrac{\partial}{\partial y_j}\left(C_{ijkl}\dfrac{\partial \beta_k^1}{\partial x_l}\right)\\ \qquad -\dfrac{\partial}{\partial x_j}\left(C_{ijkl}\dfrac{\partial \beta_k^0}{\partial x_l}\right)-k_s Gh\left(\dfrac{\partial w_0}{\partial x_i}+\dfrac{\partial w_1}{\partial y_i}-\beta_i^0\right)=0.\end{cases} \tag{12}$$

From (11), the first-order correctors w_1 and β_k^1 are defined as

$$w_1(\mathbf{x},\mathbf{y})=N_{\alpha_1}(\mathbf{y})\left(\frac{\partial w_0(\mathbf{x})}{\partial x_{\alpha_1}}-\beta_{\alpha_1}^0(\mathbf{x})\right),\quad \beta_k^1(\mathbf{x},\mathbf{y})=N_{\alpha_1 km}(\mathbf{y})\frac{\partial \beta_m^0(\mathbf{x})}{\partial x_{\alpha_1}}, \tag{13}$$

where the first-order cell functions N_{α_1} and $N_{\alpha_1 km}$ are solutions to the following boundary value problems:

$$\begin{cases} -\dfrac{\partial}{\partial y_i}\left(k_s Gh\dfrac{\partial N_{\alpha_1}}{\partial y_i}\right)=\dfrac{\partial}{\partial y_{\alpha_1}}(k_s Gh) & \text{in } Y,\\ \displaystyle\int_Y N_{\alpha_1}(\mathbf{y})d\mathbf{y}=0, \end{cases} \tag{14}$$

$$\begin{cases} -\dfrac{\partial}{\partial y_j}\left(C_{ijkl}\dfrac{\partial N_{\alpha_1 km}}{\partial y_l}\right)=\dfrac{\partial}{\partial y_j}(C_{ijm\alpha_1}) & \text{in } Y,\\ \displaystyle\int_Y N_{\alpha_1 km}(\mathbf{y})d\mathbf{y}=0. \end{cases} \tag{15}$$

Next, taking the integral average over the unit cell Y in (12), and using the newly defined expressions for w_1 and β_k^1 from (13), the homogenized Mindlin plate problem can be defined as follows:

$$\begin{cases} -\dfrac{\partial}{\partial x_i}\left(k_s G_{ij}^0 h\left(\dfrac{\partial w_0}{\partial x_j}-\beta_j^0\right)\right)=q_{\mathrm{M}}^0 & \text{in } \Omega,\\ -\dfrac{\partial}{\partial x_j}\left(C_{ijkl}^0\dfrac{\partial \beta_k^0}{\partial x_l}\right)-k_s G_{ij}^0 h\left(\dfrac{\partial w_0}{\partial x_j}-\beta_j^0\right)=0 & \text{in } \Omega,\\ w_0=0 & \text{on } \partial\Omega,\\ \beta_i^0=0 & \text{on } \partial\Omega, \end{cases} \tag{16}$$

where the homogenized coefficients G_{ij}^0 and C_{ijkl}^0, and the homogenized load q_{M}^0 are given by

$$\begin{aligned} &G_{ij}^0=\frac{1}{|Y|}\int_Y G\left(\delta_{ij}+\frac{\partial N_j}{\partial y_i}\right)d\mathbf{y},\quad C_{ijkl}^0=\frac{1}{|Y|}\int_Y\left(C_{ijkl}+C_{ijmn}\frac{\partial N_{lmk}}{\partial y_n}\right)d\mathbf{y},\\ &q_{\mathrm{M}}^0=\frac{1}{|Y|}\int_Y q_{\mathrm{M}}d\mathbf{y}, \end{aligned} \tag{17}$$

respectively, where $|Y|$ is the measure of the domain Y.

 doi:10.20944/preprints202510.0731.v1

A high-order expansion is necessary to capture the local oscillation behavior of deflection and rotation. By substituting the homogenized equation (16) and the first-order expansion (13) into (12), the second-order correctors w_2 and β_k^2 have the following expressions:

$$
\begin{aligned}
w_2(\mathbf{x},\mathbf{y}) &= N_{\alpha_1\alpha_2}(\mathbf{y})\left(\frac{\partial^2 w_0(\mathbf{x})}{\partial x_{\alpha_1}\partial x_{\alpha_2}} - \frac{\partial \beta^0_{\alpha_1}(\mathbf{x})}{\partial x_{\alpha_2}}\right) - M_{\alpha_1\alpha_2}(\mathbf{y})\frac{\partial \beta^0_{\alpha_2}(\mathbf{x})}{\partial x_{\alpha_1}},\\
\beta_k^2(\mathbf{x},\mathbf{y}) &= N_{\alpha_1\alpha_2 km}(\mathbf{y})\frac{\partial^2 \beta^0_m(\mathbf{x})}{\partial x_{\alpha_1}\partial x_{\alpha_2}} + L_{\alpha_1 k}(\mathbf{y})\left(\frac{\partial w_0(\mathbf{x})}{\partial x_{\alpha_1}} - \beta^0_{\alpha_1}(\mathbf{x})\right),
\end{aligned}
\tag{18}
$$

where the second-order cell functions $N_{\alpha_1\alpha_2}$, $M_{\alpha_1\alpha_2}$, $N_{\alpha_1\alpha_2 km}$, and $L_{\alpha_1 k}$ are solutions to the following cell problems:

$$
\begin{cases}
-\dfrac{\partial}{\partial y_i}\left(k_s G h \dfrac{\partial N_{\alpha_1\alpha_2}}{\partial y_i}\right) = \dfrac{\partial}{\partial y_{\alpha_2}}(k_s G h N_{\alpha_1}) + k_s G h \dfrac{\partial N_{\alpha_1}}{\partial y_{\alpha_2}} + k_s G h \delta_{\alpha_1\alpha_2} - k_s G^0_{\alpha_1\alpha_2} h \dfrac{q_{\mathrm{M}}}{q^0_{\mathrm{M}}} & \text{in } Y,\\
\displaystyle\int_Y N_{\alpha_1\alpha_2}(\mathbf{y})d\mathbf{y} = 0,
\end{cases}
$$

$$
\begin{cases}
-\dfrac{\partial}{\partial y_i}\left(k_s G h \dfrac{\partial M_{\alpha_1\alpha_2}}{\partial y_i}\right) = \dfrac{\partial}{\partial y_i}(k_s G h N_{\alpha_1 i\alpha_2}) & \text{in } Y,\\
\displaystyle\int_Y M_{\alpha_1\alpha_2}(\mathbf{y})d\mathbf{y} = 0,
\end{cases}
$$

$$
\begin{cases}
-\dfrac{\partial}{\partial y_j}\left(C_{ijkl} \dfrac{\partial N_{\alpha_1\alpha_2 km}}{\partial y_l}\right) = \dfrac{\partial}{\partial y_j}\left(C_{ijk\alpha_2} N_{\alpha_1 km}\right) + C_{i\alpha_2 kl}\dfrac{\partial N_{\alpha_1 km}}{\partial y_l} + C_{i\alpha_2 m\alpha_1} - C^0_{i\alpha_2 m\alpha_1} & \text{in } Y,\\
\displaystyle\int_Y N_{\alpha_1\alpha_2 km}(\mathbf{y})d\mathbf{y} = 0,
\end{cases}
$$

$$
\begin{cases}
-\dfrac{\partial}{\partial y_j}\left(C_{ijkl} \dfrac{\partial L_{\alpha_1 k}}{\partial y_l}\right) = k_s G h \delta_{i\alpha_1} + k_s G h \dfrac{\partial N_{\alpha_1}}{\partial y_i} - k_s G^0_{i\alpha_1} h & \text{in } Y,\\
\displaystyle\int_Y L_{\alpha_1 k}(\mathbf{y})d\mathbf{y} = 0,
\end{cases}
$$

Next, we move to the Timoshenko beam problem (8). Based on the results from the Mindlin plate problem, the expansions of w^ε and β^ε can be directly obtained as

$$
\begin{aligned}
w^\varepsilon(x_1) =& w_0(x_1) + \varepsilon w_1(x_1,y_1) + \varepsilon^2 w_2(x_1,y_1) + O(\varepsilon^3),\\
=& w_0(x_1) + \varepsilon N_1(y_1)\left(\frac{dw_0(x_1)}{dx_1} - \beta^0(x_1)\right) + \varepsilon^2\left(N_{11}(y_1)\frac{d^2 w_0(x_1)}{dx_1^2} + M(y_1)\frac{d\beta^0(x_1)}{dx_1}\right)\\
&+ O(\varepsilon^3),\\
\beta^\varepsilon(x_1) =& \beta^0(x_1) + \varepsilon\beta^1(x_1,y_1) + \varepsilon^2\beta^2(x_1,y_1) + O(\varepsilon^3),\\
=& \beta^0(x_1) + \varepsilon H_1(y_1)\frac{d\beta^0(x_1)}{dx_1} + \varepsilon^2\left(H_{11}(y_1)\left(\beta^0(x_1) - \frac{dw_0(x_1)}{dx_1}\right) + M_{11}(y_1)\frac{d^2\beta^0(x_1)}{dx_1^2}\right)\\
&+ O(\varepsilon^3),
\end{aligned}
\tag{19}
$$

where the first-order cell functions $N_1(y_1)$ and $H_1(y_1)$ respectively satisfy the following problems:

$$
\begin{cases}
-\dfrac{d}{dy_1}\left(k_s G A \dfrac{dN_1}{dy_1}\right) = \dfrac{d}{dy_1}(k_s G A) & \text{in } Y,\\
\displaystyle\int_Y N_1(y_1)dy_1 = 0,
\end{cases}
\tag{20}
$$

$$
\begin{cases}
-\dfrac{d}{dy_1}\left(EI \dfrac{dH_1}{dy_1}\right) = \dfrac{d}{dy_1}(EI) & \text{in } Y,\\
\displaystyle\int_Y H_1(y_1)dy_1 = 0,
\end{cases}
\tag{21}
$$

doi:10.20944/preprints202510.0731.v1

The homogenized solutions w_0 and β^0 are obtained from

$$\begin{cases} -\dfrac{d}{dx_1}\left(k_s G^0 A\left(\dfrac{dw_0}{dx_1}-\beta^0\right)\right) = q_{\mathrm{T}}^0 & \text{in } \Omega, \\ -\dfrac{d}{dx_1}\left(E^0 I\dfrac{d\beta^0}{dx_1}\right) - k_s G^0 A\left(\dfrac{dw_0}{dx_1}-\beta^0\right) = 0 & \text{in } \Omega, \\ w_0 = 0 & \text{on } \partial\Omega, \\ \beta^0 = 0 & \text{on } \partial\Omega, \end{cases} \tag{22}$$

where the homogenized coefficients G^0 and E^0, and q_{T}^0 from (22) are respectively defined by

$$G^0 = \frac{1}{|Y|}\int_Y G\left(1+\frac{dN_1}{dy_1}\right)dy_1, \quad E^0 = \frac{1}{|Y|}\int_Y E\left(1+\frac{dH_1}{dy_1}\right)dy_1, \quad q_{\mathrm{T}}^0 = \frac{1}{|Y|}\int_Y q_{\mathrm{T}}dy_1. \tag{23}$$

The second-order cell functions $N_{11}(y_1)$, $M(y_1)$, $H_{11}(y_1)$, and $M_{11}(y_1)$ are solutions to the problems:

$$\begin{cases} -\dfrac{d}{dy_1}\left(k_s GA\dfrac{dN_{11}}{dy_1}\right) = k_s GA\dfrac{dN_1}{dy_1} + \dfrac{d}{dy_1}(k_s GAN_1) + k_s GA - k_s G^0 A\dfrac{q_{\mathrm{T}}}{q_{\mathrm{T}}^0} & \text{in } Y, \\ \displaystyle\int_Y N_{11}(y_1)dy_1 = 0, \end{cases}$$

$$\begin{cases} -\dfrac{d}{dy_1}\left(k_s GA\dfrac{dM}{dy_1}\right) = \dfrac{d}{dy_1}(k_s GAN_1) + \dfrac{d}{dy_1}(k_s GAH_1) & \text{in } Y, \\ \displaystyle\int_Y M(y_1)dy_1 = 0, \end{cases}$$

$$\begin{cases} -\dfrac{d}{dy_1}\left(EI\dfrac{dH_{11}}{dy_1}\right) = -k_s GA\left(\dfrac{dN_1}{dy_1}+1\right) + k_s G^0 A & \text{in } Y, \\ \displaystyle\int_Y H_{11}(y_1)dy_1 = 0, \end{cases}$$

$$\begin{cases} -\dfrac{d}{dy_1}\left(EI\dfrac{dM_{11}}{dy_1}\right) = EI\dfrac{dH_1}{dy_1} + \dfrac{d}{dy_1}(EIH_1) + EI - E^0 I & \text{in } Y, \\ \displaystyle\int_Y M_{11}(y_1)dy_1 = 0. \end{cases}$$

4. Multi-Scale Finite Element Algorithm

According to the expansions of the deflections and rotations, we can establish the finite element(FE) algorithms for the plate and beam problems. The multiscale computational flowchart for Mindlin plate is shown in Figure 2. Two kinds of meshes are generated before the multiscale computations: cell mesh and homogenized mesh. All the cell functions are solved on the cell mesh, and the homogenized solutions are obtained on the homogenized mesh. First, let us define the first-order and second-order approximate solutions as follows:

$$\begin{aligned} &w^{\varepsilon,1} = w_0 + \varepsilon w_1, \quad w^{\varepsilon,2} = w^{\varepsilon,1} + \varepsilon^2 w_2, \\ &\beta_i^{\varepsilon,1} = \beta_i^0 + \varepsilon\beta_i^1, \quad \beta_i^{\varepsilon,2} = \beta_i^{\varepsilon,1} + \varepsilon^2\beta_i^2, \end{aligned} \tag{24}$$

 doi:10.20944/preprints202510.0731.v1

with the homogenized shear stresses V_i^0 and the first-order and second-order approximate shear stresses $V_i^{\varepsilon,1}$ and $V_i^{\varepsilon,2}$, respectively, given by

$$\begin{aligned} V_i^0 &= \frac{E^\varepsilon k_s h}{2(1+\nu^\varepsilon)}\left(\frac{\partial w_0}{\partial x_i} - \beta_0\right), \\ V_i^{\varepsilon,1} &= V_i^0 + \varepsilon \frac{E^\varepsilon k_s h}{2(1+\nu^\varepsilon)}\left(\frac{\partial w_1}{\partial x_i} - \beta_i^1\right), \\ V_i^{\varepsilon,2} &= V_i^{\varepsilon,1} + \varepsilon^2 \frac{E^\varepsilon k_s h}{2(1+\nu^\varepsilon)}\left(\frac{\partial w_2}{\partial x_i} - \beta_i^2\right). \end{aligned} \tag{25}$$

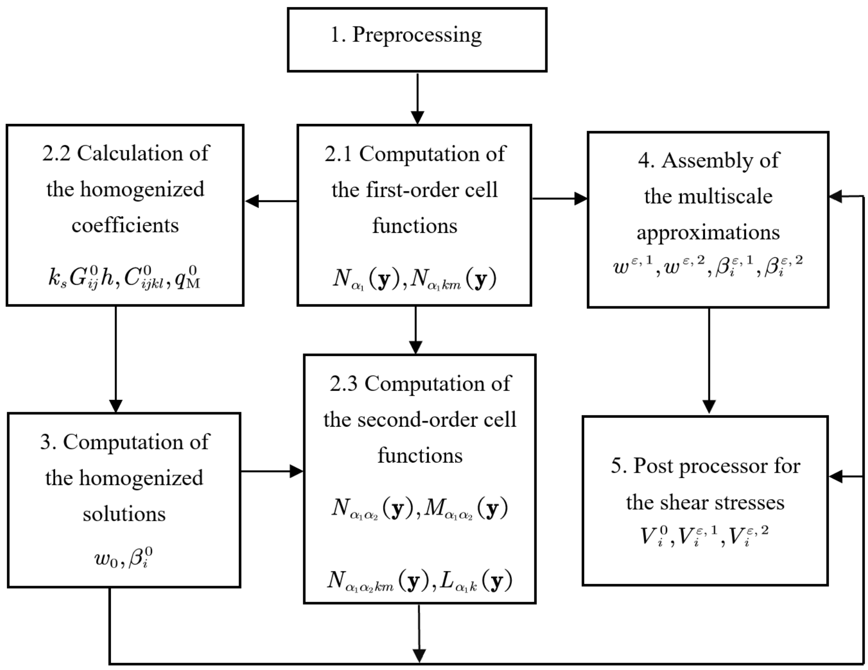

Figure 2. Finite element procedure of SOTS for the Mindlin plate problem.

The FE procedures for plate problem are illustrated as follows:

1. Preprocessing: Set the material coefficients E^ε and ν^ε, define the periodic cell Y and the homogenized domain Ω, perform the spatial discretization and generate the computational meshes. To illustrate the efficiency of the SOTS model proposed in this paper, we also partition a sufficiently refined mesh and conduct the classical computations for w^ε and β_i^ε as the reference solution for comparison.

2. Computations of the cell functions:

(1) Solve the first-order cell functions $N_{\alpha_1}(\mathbf{y})$ and $N_{\alpha_1 km}(\mathbf{y})$ based on Eqs. (14) and (15).

(2) Calculate the homogenized coefficients G_{ij}^0, C_{ijkl}^0, and q_M^0 from Eq (17).

(3) Solve the second-order cell functions $N_{\alpha_1\alpha_2}(\mathbf{y})$, $M_{\alpha_1\alpha_2}(\mathbf{y})$, $N_{\alpha_1\alpha_2 km}(\mathbf{y})$, and $L_{\alpha_1 k}(\mathbf{y})$.

3. Computations of the homogenized solutions w_0 and β_i^0.

4. Assembly of the first-order and second-order multiscale approximations $w^{\varepsilon,1}$, $w^{\varepsilon,2}$, $\beta_i^{\varepsilon,1}$, and $\beta_i^{\varepsilon,2}$ from Eq (24) in an incremental way.

5. Postprocessing: Compute the first-order and second-order multiscale approximate shear stresses: V_i^0, $V_i^{\varepsilon,1}$, and $V_i^{\varepsilon,2}$ based on Eq (25).

As is well known, the effects of shear deformations become negligible as the thickness decreases. To address this, consistent interpolation element (CIE) is employed to solve the plate problem.

To evaluate the accuracy of the proposed asymptotic model, the relative errors are defined by

 doi:10.20944/preprints202510.0731.v1

$$e_w^{\varepsilon,i} = \frac{\|w^\varepsilon - w^{\varepsilon,i}\|_{L^2(\Omega)}}{\|w^\varepsilon\|_{L^2(\Omega)}}, \quad e_{\beta_1}^{\varepsilon,i} = \frac{\left\|\beta_1^\varepsilon - \beta_1^{\varepsilon,i}\right\|_{L^2(\Omega)}}{\|\beta_1^\varepsilon\|_{L^2(\Omega)}}, \quad e_{\beta_2}^{\varepsilon,i} = \frac{\left\|\beta_2^\varepsilon - \beta_2^{\varepsilon,i}\right\|_{L^2(\Omega)}}{\|\beta_2^\varepsilon\|_{L^2(\Omega)}}, \quad i = 0, 1, 2, \tag{26}$$

where $w^{\varepsilon,0} = w_0$, $\beta_1^{\varepsilon,0} = \beta_1^0$, and $\beta_2^{\varepsilon,0} = \beta_2^0$.

5. Numerical Examples

5.1. Multi-Scale Approximation for Plate Problem

The SOTS asymptotic expansion method is applied to Mindlin plates made of various composite materials. Several numerical examples are provided to test the accuracy of the proposed algorithm.

5.1.1. Composite Mindlin Plate

Consider a square plate of length $L = 1$m with thickness $h = 0.2$m, clamped on all sides and subjected to a uniform load $q_M = 1.0 \times 10^6$ kN. The macro region and representative cell are shown in Figure 3 (a) and (b), respectively. Let material a_1 be carbon steel with $E^\varepsilon = 200$GPa and $\nu^\varepsilon = 0.25$, and material a_2 be low-density polyethylene(LDPE) with $E^\varepsilon = 0.3$GPa and $\nu^\varepsilon = 0.49$. The shear correction factor $k_s = 0.833$ is adopted for both materials. ε is chosen as 2^{-k}, $k = 2, .., 7$. The mesh information for the classical FE computations and SOTS approximation is listed in Table 1. It is evident that the classical computations take a significant amount of computational time while the proposed SOTS asymptotic method requires calculations only on a single cell and a homogenization domain with much less CPU time and also memory requirement. The relative L^2-errors of the approximation solutions are displayed in Table 2, which can be seen that the errors decreases as ε becomes small.

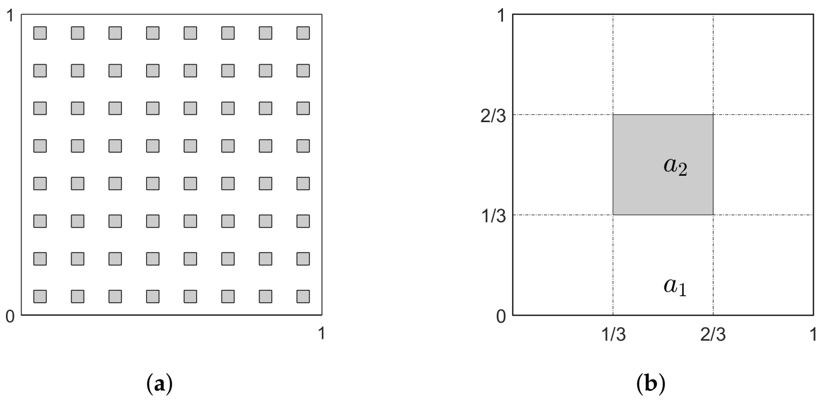

Figure 3. Macro domain Ω and cell domain Y with constituent materials a_1 and a_2 ($\varepsilon = \frac{1}{8}$). **(a)** Macroscopic domain Ω; **(b)** Microscopic cell domain Y.

The convergence curves of deflection and rotations with respect to ε are presented in Figure 4. It is observed that the convergence orders for w^ε and β_i^ε are approximately $\mathcal{O}(\varepsilon^2)$ and $\mathcal{O}(\varepsilon^1)$, respectively. Due to all the cell functions and homogenized solutions have to be mapped into the fine meshes with different ε. The interpolations errors between the cell mesh, homogenized mesh and the fine meshes as well as the numerical differential errors for computing the high-order derivatives of the homogenized solutions influence the relative errors computations, which to some extent conceal the convergence order of the asymptotic models.

doi:10.20944/preprints202510.0731.v1

Table 1. Mesh information and CPU time for general FE and SOTS asymptotic computation.

	Classical FE computation $\Omega(\varepsilon)$						Two-scale computation	
	$\frac{1}{4}$	$\frac{1}{8}$	$\frac{1}{16}$	$\frac{1}{32}$	$\frac{1}{64}$	$\frac{1}{128}$	Y	Ω
FE Nodes	2921	11537	45857	182849	730241	2918657	197	12321
FE Elements	5696	22784	91136	364544	1458176	5832704	356	24200
CPU Time(s)	0.988	3.539	18.313	74.263	622.632	5501.666	0.093	8.578

Table 2. Computed relative L^2-errors for the Mindlin plate with different ε.

ε	$e_w^{\varepsilon,0}$	$e_w^{\varepsilon,1}$	$e_w^{\varepsilon,2}$	$e_{\beta_1}^{\varepsilon,0}$	$e_{\beta_1}^{\varepsilon,1}$	$e_{\beta_1}^{\varepsilon,2}$	$e_{\beta_2}^{\varepsilon,0}$	$e_{\beta_2}^{\varepsilon,1}$	$e_{\beta_2}^{\varepsilon,2}$
$\frac{1}{4}$	4.8002E-1	4.8032E-1	4.0015E-2	1.8134E-1	1.0996E-1	1.1268E-1	1.8159E-1	1.0997E-1	9.9784E-2
$\frac{1}{8}$	1.4407E-1	1.4375E-1	1.4428E-2	8.0707E-2	3.1478E-2	2.9195E-2	8.0852E-2	3.1478E-2	2.6609E-2
$\frac{1}{16}$	3.6506E-2	3.6172E-2	4.5398E-3	4.0564E-2	1.4067E-2	1.3478E-2	4.0605E-2	1.4028E-2	1.3113E-2
$\frac{1}{32}$	8.8193E-3	8.3226E-3	1.5738E-3	2.0023E-2	7.2921E-3	7.1350E-3	2.0044E-2	7.2757E-3	7.0789E-3
$\frac{1}{64}$	2.2198E-3	1.8241E-3	7.1274E-4	9.1498E-3	4.1504E-3	4.0925E-3	9.1432E-3	4.1134E-3	4.0514E-3
$\frac{1}{128}$	8.0502E-4	5.8576E-4	4.7236E-4	4.6591E-3	3.0136E-3	2.9979E-3	4.6346E-3	2.9669E-3	2.9514E-3

Figures 5 and 6 show the computed deflection w^ε and rotations β_i^ε when $\varepsilon = 1/8$. It is indicated that adding the second-order approximations w_2 provides a better approximation of w^ε due to the pronounced changes in deflection w. The second-order correctors β_1^2 and β_2^2 show a slight improvement over the first-order correctors β_1^1 and β_2^1, because the changes in rotation β_1^ε and β_2^ε are less obvious. Overall, the SOTS asymptotic expansions offer a more accurate representation of oscillatory behavior compared to the first-order solutions.

The approximation of the shear stresses can be obtained when $\varepsilon = \frac{1}{8}$, which is shown in Figure 7. It can be observed that the oscillations are more remarkable for the stress distributions than the displacement field (Figure 7 (a) and (e)), the homogenized solutions in Figure 7 (b) and (f) only give the macroscopic behavior and the first-order solutions in Figure 7 (c) and (g) are not capable of capturing the peak of the stress within the constituent material LDPE. Therefore, the second-order correctors are necessary to be defined and appended in the asymptotic expansions to give the satisfactory distributions, which are shown in Figure 7 (d) and (h).

Figure 8 illustrates the approximations of shear stresses along the diagonal line, and it is evident that incorporating second-order correctors provides a more accurate characterization of oscillations compared to both homogenized solutions and first-order approximations.

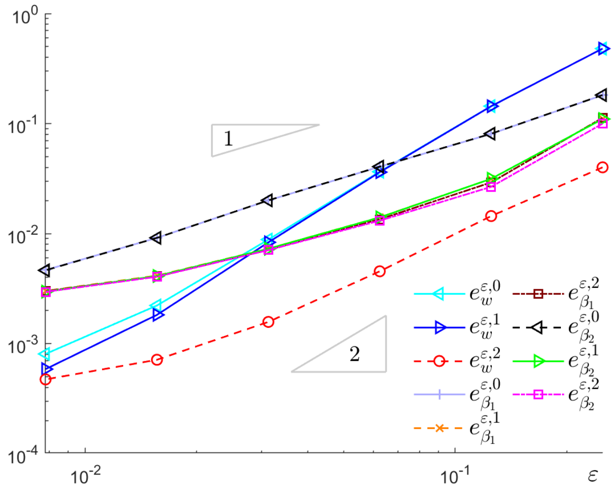

Figure 4. Convergence of the deflection and the rotations with decreasing ε.

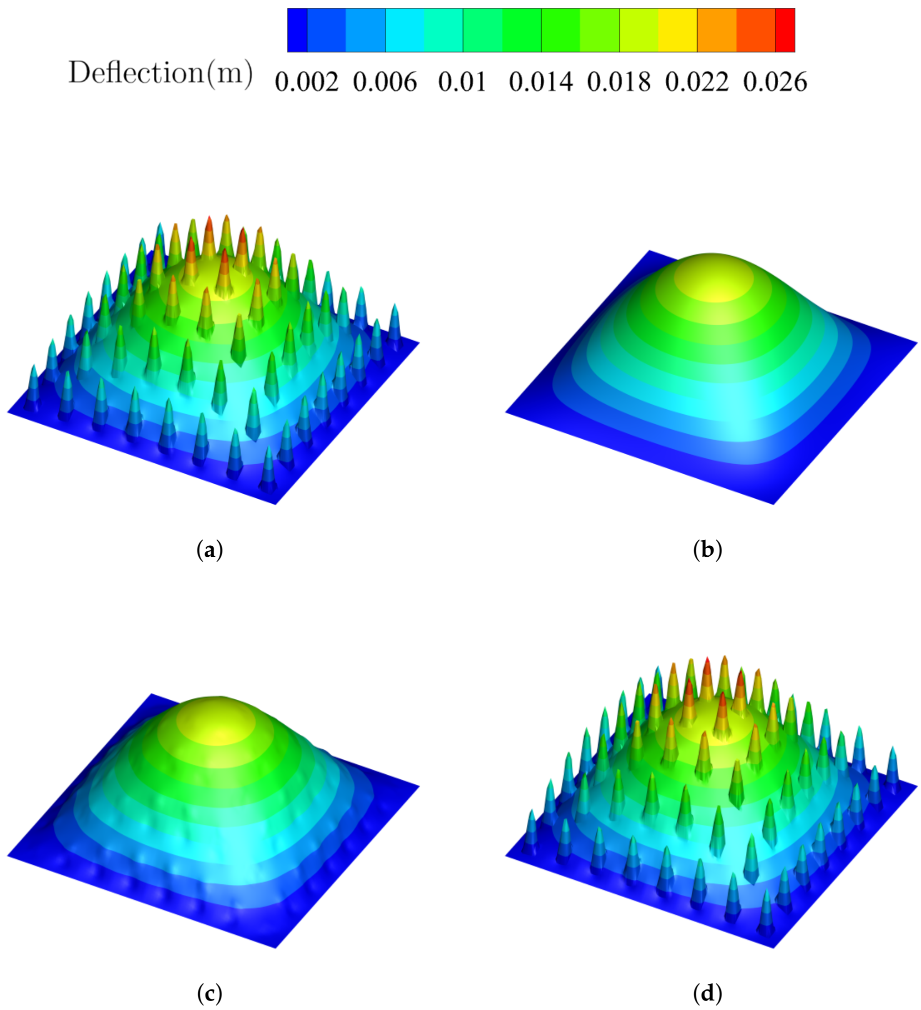

Figure 5. Approximation of the deflection w^ε by the SOTS computation ($\varepsilon = \frac{1}{8}$). **(a)** w^ε; **(b)** w_0; **(c)** $w^{\varepsilon,1}$; **(d)** $w^{\varepsilon,2}$.

doi:10.20944/preprints202510.0731.v1

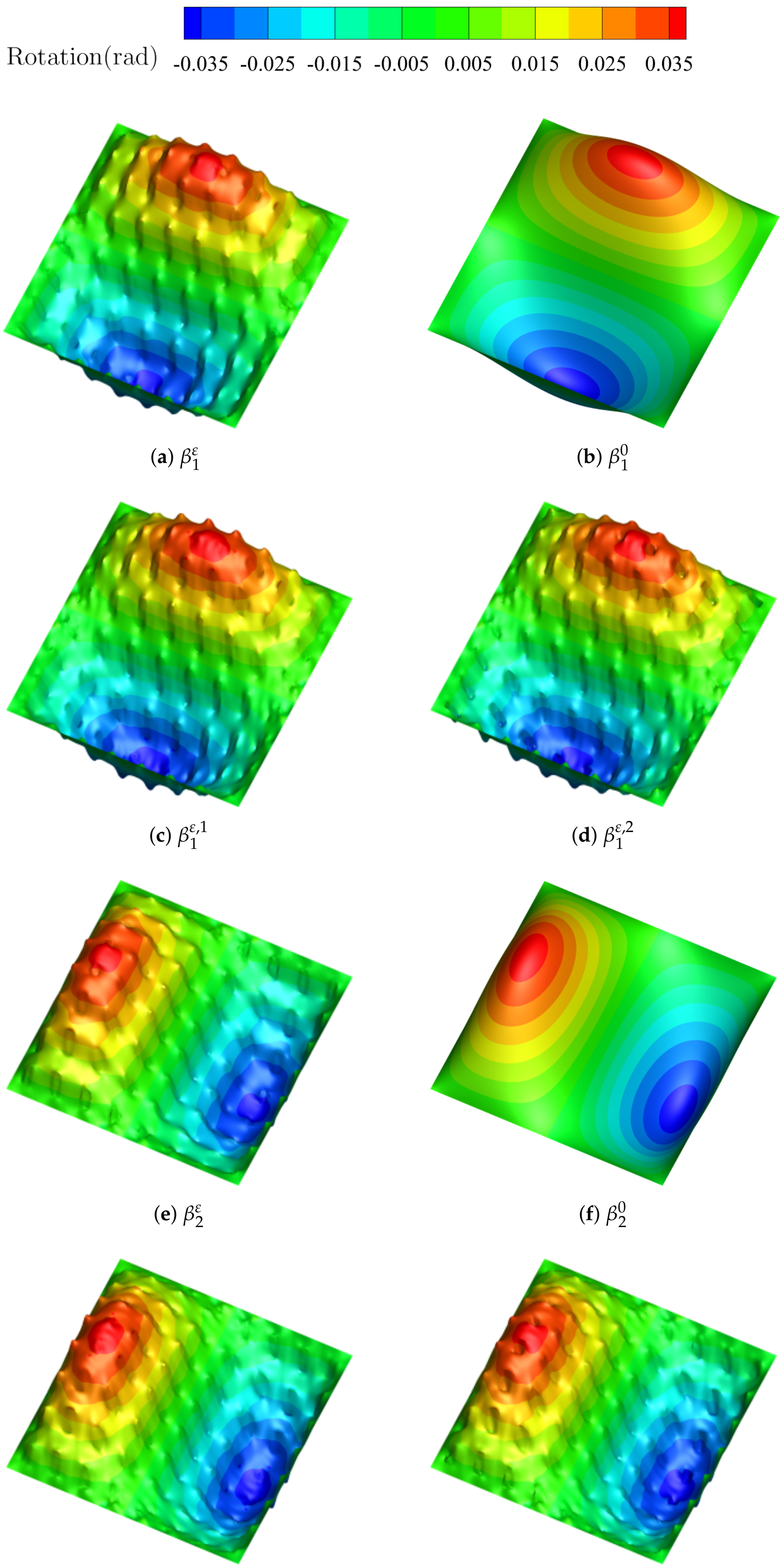

(a) β_1^ε (b) β_1^0

(c) $\beta_1^{\varepsilon,1}$ (d) $\beta_1^{\varepsilon,2}$

(e) β_2^ε (f) β_2^0

(g) $\beta_2^{\varepsilon,1}$ (h) $\beta_2^{\varepsilon,2}$

Figure 6. Approximation of the rotations β_1^ε and β_2^ε by the SOTS computation ($\varepsilon = \frac{1}{8}$). **(a)** w^ε; **(b)** w_0; **(c)** $w^{\varepsilon,1}$; **(d)** $w^{\varepsilon,2}$.

doi:10.20944/preprints202510.0731.v1

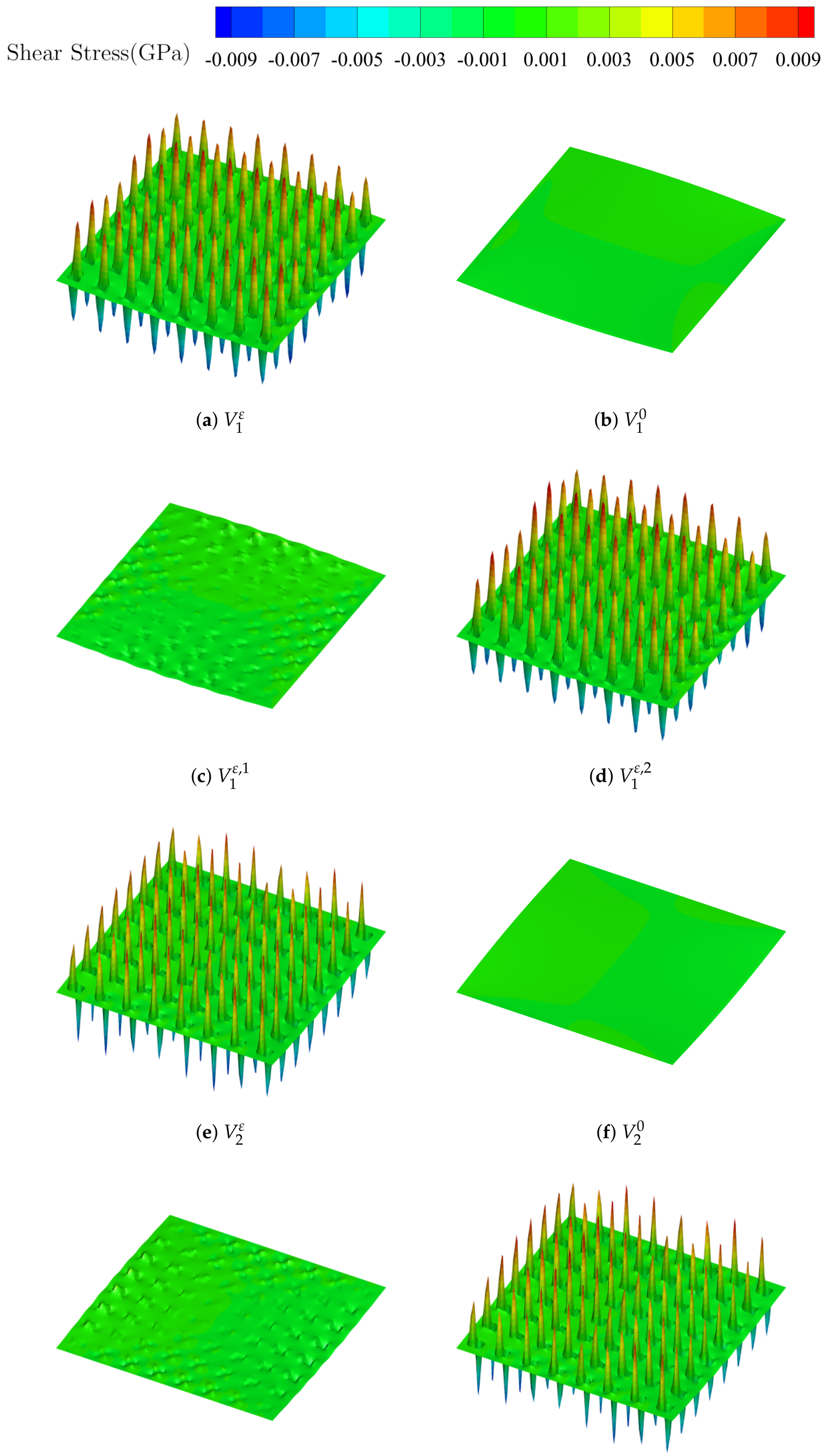

(a) V_1^ε (b) V_1^0

(c) $V_1^{\varepsilon,1}$ (d) $V_1^{\varepsilon,2}$

(e) V_2^ε (f) V_2^0

(g) $V_2^{\varepsilon,1}$ (h) $V_2^{\varepsilon,2}$

Figure 7. Approximation of the shear stresses V_1^ε and V_2^ε by the SOTS computation ($\varepsilon = \frac{1}{8}$).

Preprints.org (www.preprints.org) | NOT PEER-REVIEWED | Posted: 10 October 2025 doi:10.20944/preprints202510.0731.v1

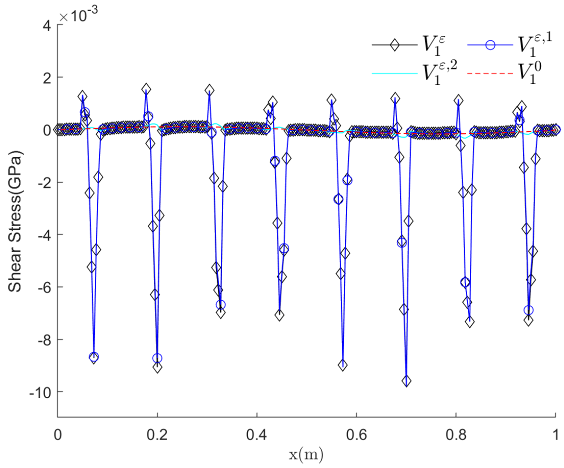

(a) V_1^ε

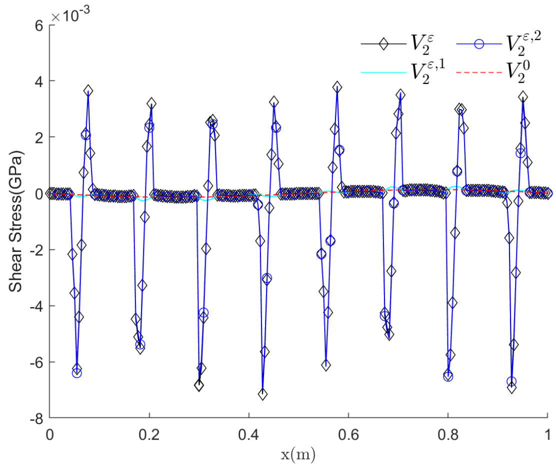

(b) V_2^ε

Figure 8. Approximation of the shear stresses V_1^ε and V_2^ε along the diagonal line ($\varepsilon = \frac{1}{8}$).

5.1.2. Convergence for Kirchhoff Plate

Next, we check if the asymptotic model is also effective to describe the behavior of the Kirchhoff plate. Consider also a clamped square plate with a uniform load $q_M = 1.0 \times 10^3$ kN. The material parameter in a_1 and a_2 is the same as in [24]. For the macroscopic domain and each microscopic cell, divide the domain into 80×80 squares and 50 triangles for calculations.

To quantify the convergence behavior of the composite plate, w_K, $\beta_{1,K}$, and $\beta_{2,K}$ are computed using the discrete Kirchhoff theory. The computed relative L^2-errors are given by:

$$e_{w,K}^{\varepsilon,i} = \frac{\left\| w^{\varepsilon,i} - w_K \right\|_{L^2(\Omega)}}{\left\| w_K \right\|_{L^2(\Omega)}}, \quad e_{\beta_1,K}^{\varepsilon,i} = \frac{\left\| \beta_1^{\varepsilon,i} - \beta_{1,K} \right\|_{L^2(\Omega)}}{\left\| \beta_{1,K} \right\|_{L^2(\Omega)}}, \quad e_{\beta_2,K}^{\varepsilon,i} = \frac{\left\| \beta_2^{\varepsilon,i} - \beta_{2,K} \right\|_{L^2(\Omega)}}{\left\| \beta_{2,K} \right\|_{L^2(\Omega)}}. \tag{27}$$

Let h/L be 0.2, 0.1, and 0.035, respectively. Perform traditional FE computation for the Kirchhoff plate and compare these with asymptotic solutions. Although the plate model exhibits no significant shear locking, implementation of the CIE method is still required to prevent potential locking effects. Tables 3, 4, and 5 present the relative L^2-errors for different ε. It is observed that β_1^ε and β_2^ε of the Mindlin plate converge to $\beta_{1,K}$ and $\beta_{2,K}$, while w^ε approaches w_K as h decreases. The deflection w_K can be approximated by w_0 when h is not small, whereas $w^{\varepsilon,2}$ provides a more accurate approximation when h decreases. Due to the relatively smooth variation in w_K, $w^{\varepsilon,2}$ shows only a limited improvement in accuracy compared with w_0 and $w^{\varepsilon,1}$. $\beta_{1,K}$ and $\beta_{2,K}$ are best approximated by appending β_1^2 and β_2^2, which can also be shown in Figures 9 and 10.

Table 3. Composite Mindlin plate approaching the composite Kirchhoff plate ($h/L = 0.2$).

ε	$e_{w,K}^{\varepsilon,0}$	$e_{w,K}^{\varepsilon,1}$	$e_{w,K}^{\varepsilon,2}$	$e_{\beta_1,K}^{\varepsilon,0}$	$e_{\beta_1,K}^{\varepsilon,1}$	$e_{\beta_1,K}^{\varepsilon,2}$	$e_{\beta_2,K}^{\varepsilon,0}$	$e_{\beta_2,K}^{\varepsilon,1}$	$e_{\beta_2,K}^{\varepsilon,2}$
$\frac{1}{4}$	1.1271	1.1270	1.1363	2.4425E-1	2.4039E-1	2.3275E-1	2.4422E-1	2.4035E-1	2.3274E-1
$\frac{1}{8}$	7.7704E-1	7.7707E-1	7.7860E-1	1.4543E-1	1.3928E-1	1.3810E-1	1.4543E-1	1.3932E-1	1.3812E-1
$\frac{1}{16}$	8.4653E-1	8.4654E-1	8.4700E-1	1.4078E-1	1.3938E-1	1.3937E-1	1.4078E-1	1.3938E-1	1.3937E-1
$\frac{1}{24}$	8.4770E-1	8.4771E-1	8.4791E-1	1.3969E-1	1.3929E-1	1.3928E-1	1.3969E-1	1.3929E-1	1.3928E-1

Preprints.org (www.preprints.org) | NOT PEER-REVIEWED | Posted: 10 October 2025 doi:10.20944/preprints202510.0731.v1

Table 4. Composite Mindlin plate approaching the composite Kirchhoff plate ($h/L = 0.1$).

ε	$e^{\varepsilon,0}_{w,K}$	$e^{\varepsilon,1}_{w,K}$	$e^{\varepsilon,2}_{w,K}$	$e^{\varepsilon,0}_{\beta_1,K}$	$e^{\varepsilon,1}_{\beta_1,K}$	$e^{\varepsilon,2}_{\beta_1,K}$	$e^{\varepsilon,0}_{\beta_2,K}$	$e^{\varepsilon,1}_{\beta_2,K}$	$e^{\varepsilon,2}_{\beta_2,K}$
$\frac{1}{4}$	3.7340E-1	3.7337E-1	3.7931E-1	1.5980E-1	1.5433E-1	1.4895E-1	1.5980E-1	1.5433E-1	1.4954E-1
$\frac{1}{8}$	1.5855E-1	1.5855E-1	1.5938E-1	9.4118E-2	8.4455E-2	7.2935E-2	9.4118E-2	8.4501E-2	7.2891E-2
$\frac{1}{16}$	2.0104E-1	2.0104E-1	2.0134E-1	6.5862E-2	6.2822E-2	6.1235E-2	6.5862E-2	6.2846E-2	6.1228E-2
$\frac{1}{24}$	2.0388E-1	2.0388E-1	2.0403E-1	6.1348E-2	6.0448E-2	5.9565E-2	6.1348E-2	6.0442E-2	5.9572E-2

Table 5. Composite Mindlin plate approaching the composite Kirchhoff plate ($h/L = 0.035$).

ε	$e^{\varepsilon,0}_{w,K}$	$e^{\varepsilon,1}_{w,K}$	$e^{\varepsilon,2}_{w,K}$	$e^{\varepsilon,0}_{\beta_1,K}$	$e^{\varepsilon,1}_{\beta_1,K}$	$e^{\varepsilon,2}_{\beta_1,K}$	$e^{\varepsilon,0}_{\beta_2,K}$	$e^{\varepsilon,1}_{\beta_2,K}$	$e^{\varepsilon,2}_{\beta_2,K}$
$\frac{1}{4}$	1.1742E-1	1.1742E-1	1.2157E-1	1.0402E-1	8.6248E-2	8.4552E-2	1.0402E-1	8.6256E-2	8.3637E-2
$\frac{1}{8}$	4.0151E-2	4.0147E-2	3.8461E-2	8.4931E-2	7.3972E-2	5.9328E-2	8.4931E-2	7.3956E-2	5.9577E-2
$\frac{1}{16}$	1.0786E-2	1.0789E-2	1.0505E-2	3.7998E-2	3.2589E-2	2.8209E-2	3.7998E-2	3.2581E-2	2.8388E-2
$\frac{1}{24}$	8.4341E-3	8.4346E-3	8.3463E-3	3.0168E-2	2.8329E-2	2.5397E-2	3.0168E-2	2.8321E-2	2.5489E-2

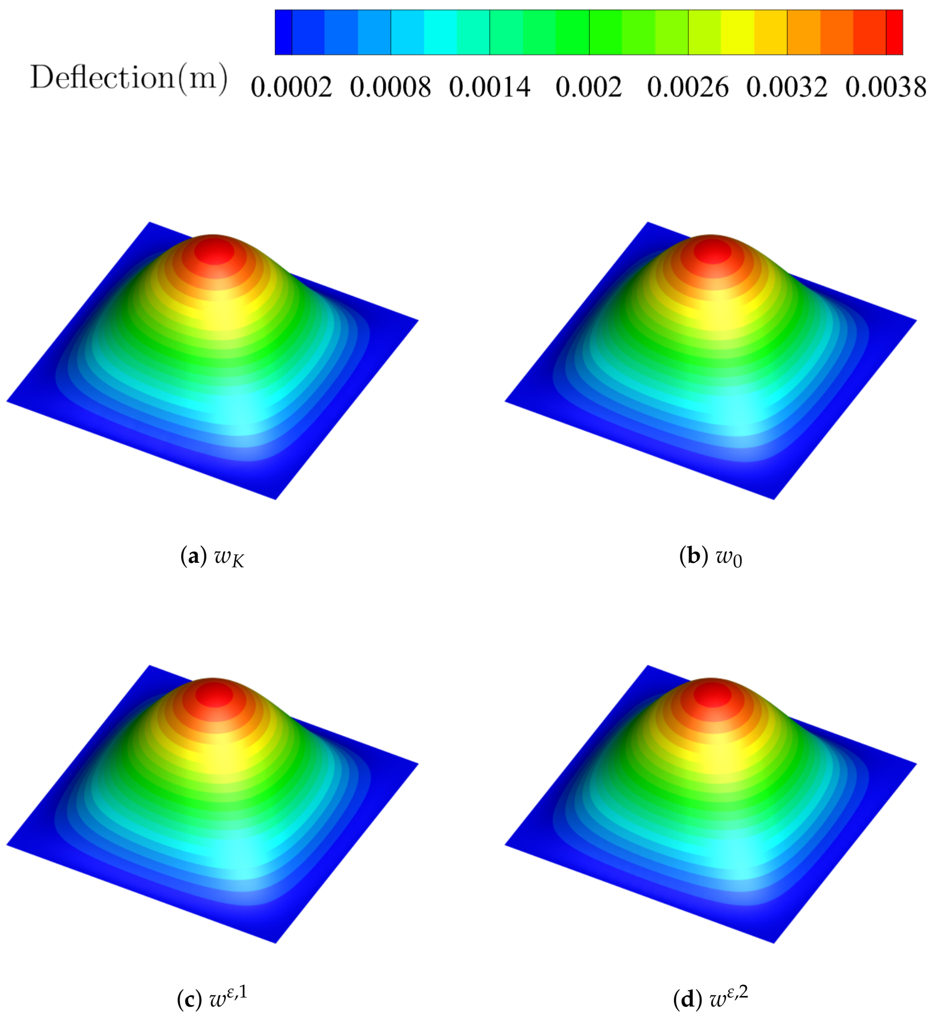

Figure 9. Approximation of the deflection w_K by the SOTS computation ($\varepsilon = 1/24$, $h/L = 0.035$).

Preprints.org (www.preprints.org) | NOT PEER-REVIEWED | Posted: 10 October 2025 doi:10.20944/preprints202510.0731.v1

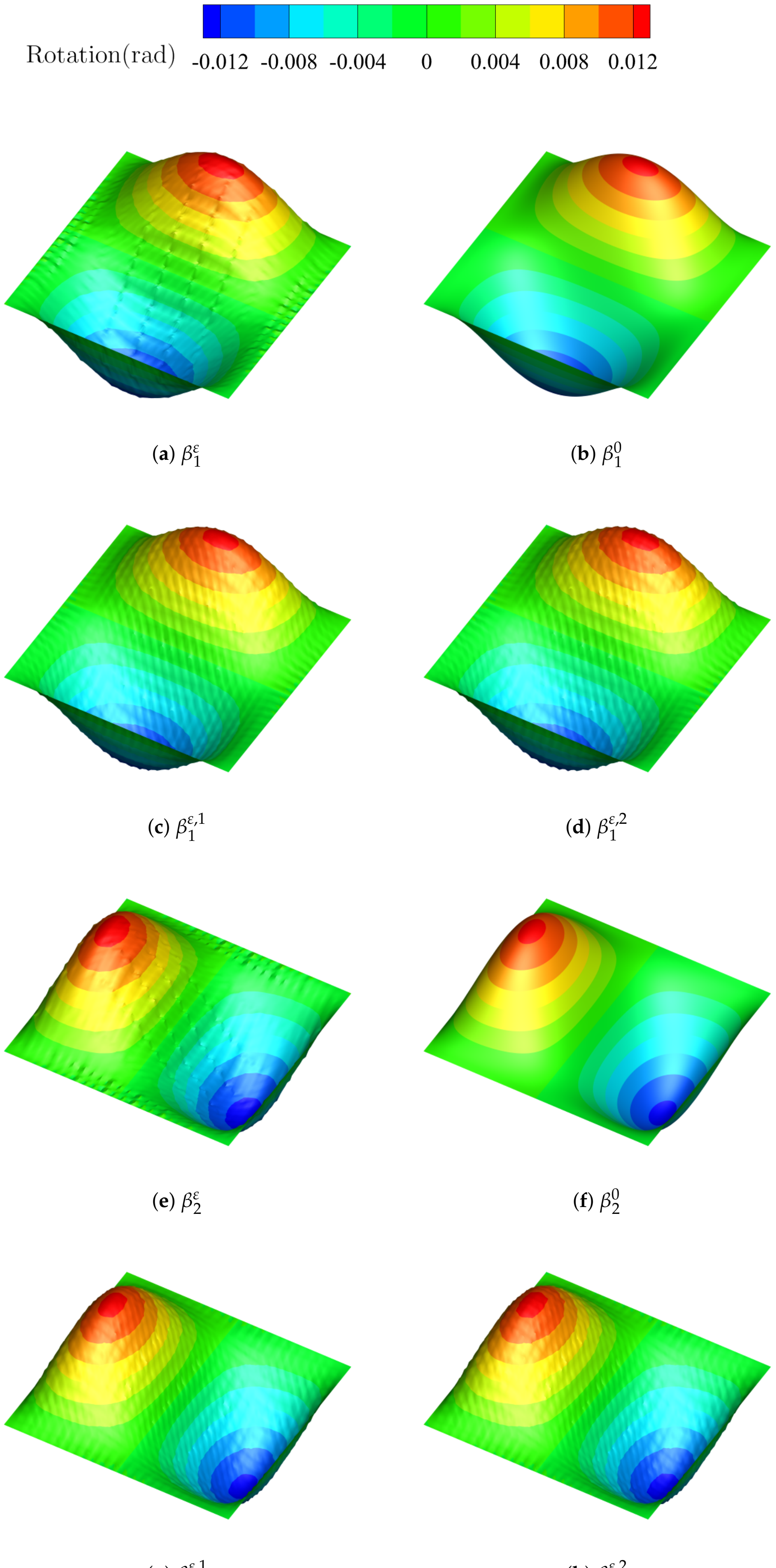

(a) β_1^{ε} (b) β_1^{0}

(c) $\beta_1^{\varepsilon,1}$ (d) $\beta_1^{\varepsilon,2}$

(e) β_2^{ε} (f) β_2^{0}

(g) $\beta_2^{\varepsilon,1}$ (h) $\beta_2^{\varepsilon,2}$

Figure 10. Approximation of the rotations $\beta_{1,K}$ and $\beta_{2,K}$ by the SOTS computation ($\varepsilon = 1/24$, $h/L = 0.035$).

doi:10.20944/preprints202510.0731.v1

A comparison with the numerical example in [24] is performed to validate the rationality of the approach proposed in this paper. The unit cell has a height of 1 cm and in-plane dimensions a_2 of Y, measuring 0.3×0.3 cm^2, with a square inclusion at its center. Under the same conditions as in Example 1: Free Vibration of a CCCC Single-Layer Periodic Plate, the homogenized stiffness matrix D^0 can be

$$D^0 = \begin{bmatrix} 7.5074 & 2.0974 & 0 \\ 2.0974 & 7.5074 & 0 \\ 0 & 0 & 2.7050 \end{bmatrix} \times 10^3 \ \mathrm{N} \cdot \mathrm{m}, \tag{28}$$

which is closely matches the homogenized stiffness matrix D^H given in [24] as follows:

$$D^H = \begin{bmatrix} 7.4706 & 1.8731 & 0 \\ 1.8731 & 7.4706 & 0 \\ 0 & 0 & 2.8352 \end{bmatrix} \times 10^3 \ \mathrm{N} \cdot \mathrm{m}. \tag{29}$$

5.2. Multi-Scale Approximation for Beam Problem

The SOTS method is also utilized to analyze the composite Timoshenko beam.

5.2.1. Composite Timoshenko Beam

Consider a composite beam of unit length with width $b = 0.1$m and height $h = 0.2$m, which is clamped at both ends and subjected to a uniform load $q_T = 1.0 \times 10^5$kN. The macro and cell domains are shown in Figure 11 (a) and (b), where $\Omega_a(\Omega_b)$ is occupied by the material $y_a(y_b)$. Choose $E^\varepsilon = 17$GPa and $\nu^\varepsilon = 0.42$ for the plumbum (y_a) in Ω_a, and $E^\varepsilon = 206$GPa and $\nu^\varepsilon = 0.3$ for the alloy steel (y_b) in Ω_b. The macroscopic domain Ω is discretized into 100 finite elements for computation. Let ε be 2^{-k}, $k = 2, ..., 8$. The computed relative L^2-errors are shown in Table 6.

It is shown that the SOTS computation also offers improved precision for approximating both w^ε and β^ε with less computational effort compared to the general FE method.

The asymptotic approximations for $\varepsilon = \frac{1}{2}, \frac{1}{4}$, and $\frac{1}{8}$ are presented in Figure 12, with local detail graphs within. Compared to $\varepsilon = \frac{1}{2}$, $w^{\varepsilon,2}$ and $\beta^{\varepsilon,2}$ are gradually closer to w^ε and β^ε for $\varepsilon = \frac{1}{4}$ and $\frac{1}{8}$. As shown in the figures, the approximation for $\varepsilon = \frac{1}{8}$ is more effective compared to $\varepsilon = \frac{1}{4}$ with more details captured.

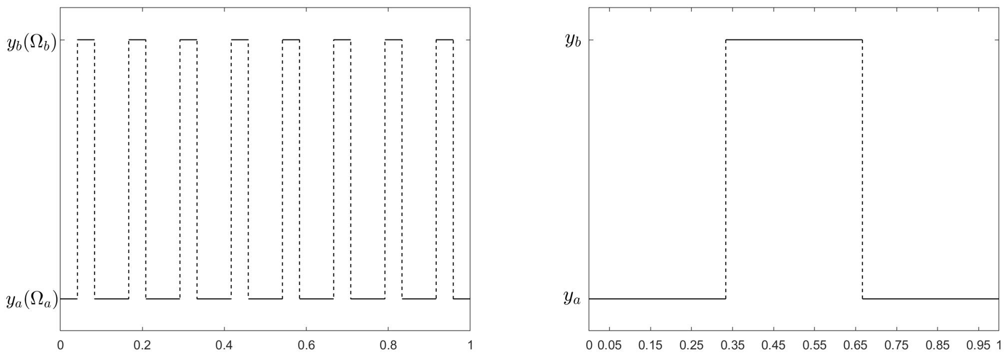

(**a**) Macroscopic domain Ω (**b**) Microscopic cell domain Y

Figure 11. Macro region Ω and single cell region Y of the beam problem ($\varepsilon = \frac{1}{8}$).

Preprints.org (www.preprints.org) | NOT PEER-REVIEWED | Posted: 10 October 2025 doi:10.20944/preprints202510.0731.v1

Table 6. Computed relative L^2 -errors for the Timoshenko beam with different ε.

ε	$e_w^{\varepsilon,0}$	$e_w^{\varepsilon,1}$	$e_w^{\varepsilon,2}$	$e_\beta^{\varepsilon,0}$	$e_\beta^{\varepsilon,1}$	$e_\beta^{\varepsilon,2}$
$\frac{1}{4}$	6.3204E-2	2.4709E-2	1.5073E-2	1.5090E-1	6.2674E-2	9.3377E-3
$\frac{1}{8}$	3.0314E-2	6.4404E-3	3.9261E-3	7.2027E-2	1.7268E-2	1.6630E-3
$\frac{1}{16}$	1.4972E-2	1.6276E-3	9.9237E-4	3.5300E-2	4.5739E-3	5.7680E-4
$\frac{1}{32}$	7.4627E-3	4.0824E-4	2.4907E-4	1.7546E-2	1.2491E-3	2.7353E-4
$\frac{1}{64}$	3.7286E-3	1.0223E-4	6.2463E-5	8.7584E-3	3.6755E-4	1.3517E-4
$\frac{1}{128}$	1.8640E-3	2.5668E-5	1.5758E-5	4.3770E-3	1.2178E-4	6.7338E-5
$\frac{1}{256}$	9.3197E-4	5.7469E-6	3.2017E-6	2.1881E-3	4.5484E-5	3.2711E-5

The converging behaviors of the deflection and the rotation with respect to ε are shown in Figure 13. It can be observed from the figure that the convergence rates for the w^ε and β^ε are approximately $\mathcal{O}(\varepsilon^2)$, whereas the convergence order of the homogenized result is approximately $\mathcal{O}(\varepsilon^1)$.

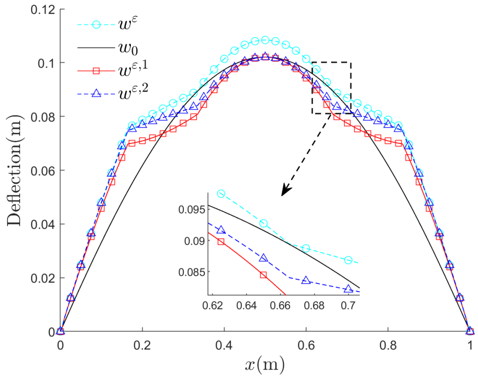

(a) $\varepsilon = \frac{1}{2}$

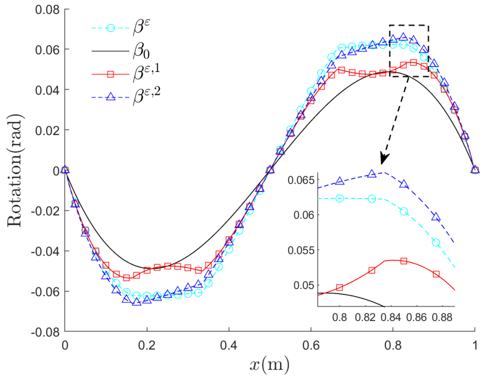

(b) $\varepsilon = \frac{1}{2}$

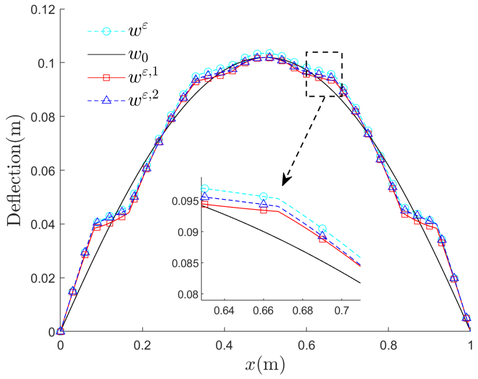

(c) $\varepsilon = \frac{1}{4}$

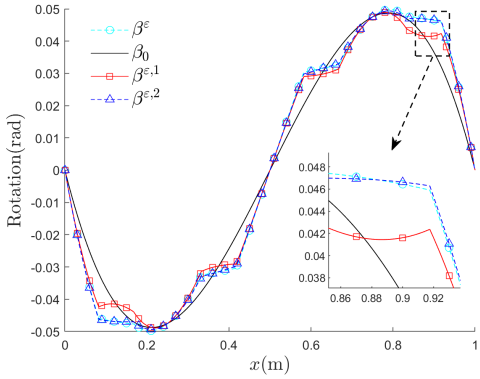

(d) $\varepsilon = \frac{1}{4}$

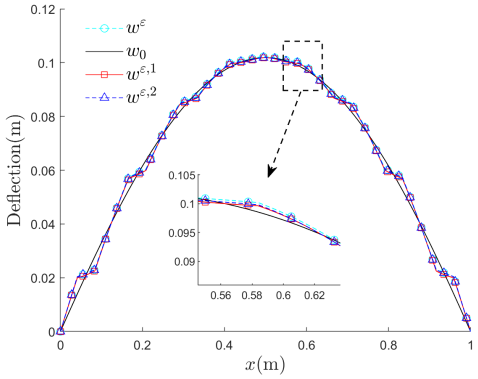

(e) $\varepsilon = \frac{1}{8}$

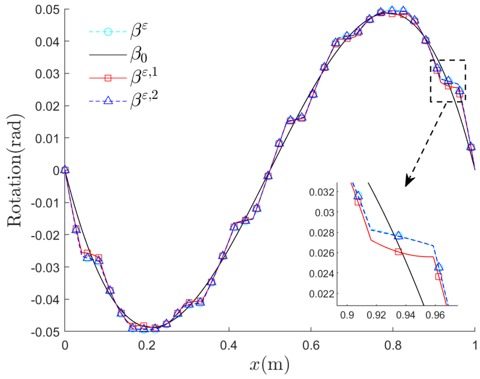

(f) $\varepsilon = \frac{1}{8}$

Figure 12. Comparison of computed deflections and rotations with $\varepsilon = \frac{1}{2}$, $\frac{1}{4}$ and $\frac{1}{8}$.

Preprints.org (www.preprints.org) | NOT PEER-REVIEWED | Posted: 10 October 2025 doi:10.20944/preprints202510.0731.v1

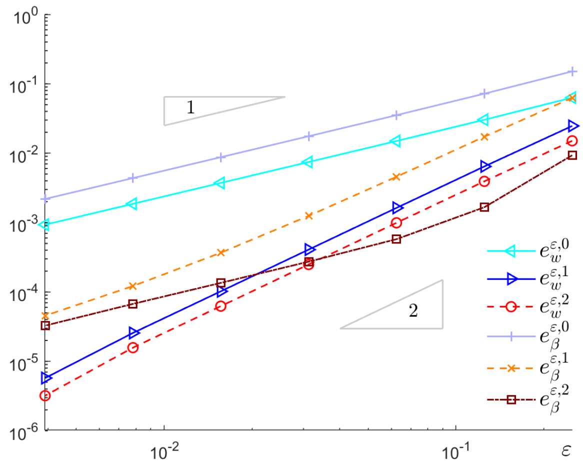

Figure 13. Convergence of the deflection and the rotation with decreasing ε.

5.2.2. Convergence for Euler Beam

Choose $q_T = 1.0 \times 10^3$ kN. As the thickness h decreases, the beam model requires finer mesh discretization. In the macroscopic domain, the domain is divided into 400 mesh elements for calculations, and other parameters are selected similarly to those in Section 5.2.1. Define w_E and β_E as the deflection and rotation of the Euler beam obtained by the general FE method. The relative L^2-errors $e^{\varepsilon,i}_{w,E}$ and $e^{\varepsilon,i}_{\beta,E}$ are defined similarly to (27).

Compare the solutions of the numerical method with the solutions w_E and β_E of the Euler beam using the general finite element method. Since the rotation β^ε of the Timoshenko beam remains close to the rotation β_E for $h = 0.1$ m, 0.035 m, and 0.02 m, while the deflection w^ε of the Timoshenko beam approximates w_E more accurately when h is small, as shown in Figure 14 (a)-(f). It is shown that approximating the deflection w_E by appending the second-order corrector w_2 is more effective than using the first-order corrector w_1 and the homogenized solution w_0, when h is small as $h = 0.035$ m and 0.02 m. The microscopic homogenized coefficients used to obtain the homogenized Euler beam are displayed as follows:

$$E^0 = 24503, \quad \nu^0 = 0.415236, \quad G^0 = 8,656.8601. \tag{30}$$

The relative L^2-errors of the homogenized Euler beam when approximating the composite Euler beam are displayed in Table 7. As ε gradually decreases, the relative errors are reduced, and approximations of both deflection and rotation improve.

Table 7. Approximation of the homogenized Euler beam ($h/L = 0.02$).

ε	$e^{\varepsilon}_{w,E,0}$	$e^{\varepsilon}_{\beta,E,0}$
$\frac{1}{4}$	9.5292E-2	1.4726E-1
$\frac{1}{8}$	2.7921E-2	7.0550E-2
$\frac{1}{16}$	4.6500E-3	3.5153E-2
$\frac{1}{24}$	2.7279E-3	2.3052E-2

Additionally, the rotation β_E is better approximated by adding the second-order corrector β_2 than using the homogenized solution β_0 or appending the first-order corrector β_1 for different values of h. This is detailed in Tables 8, 9, and 10. As h decreases from 0.1 m to 0.02 m, the composite Timoshenko beam gradually approximates the composite Euler beam more closely.

When the thickness h reaches a minimum of 0.02 m, no significant shear locking phenomenon is observed. However, when h is less than 0.001 m, pronounced shear locking occurs, necessitating the application of RIE method to address this numerical issue.

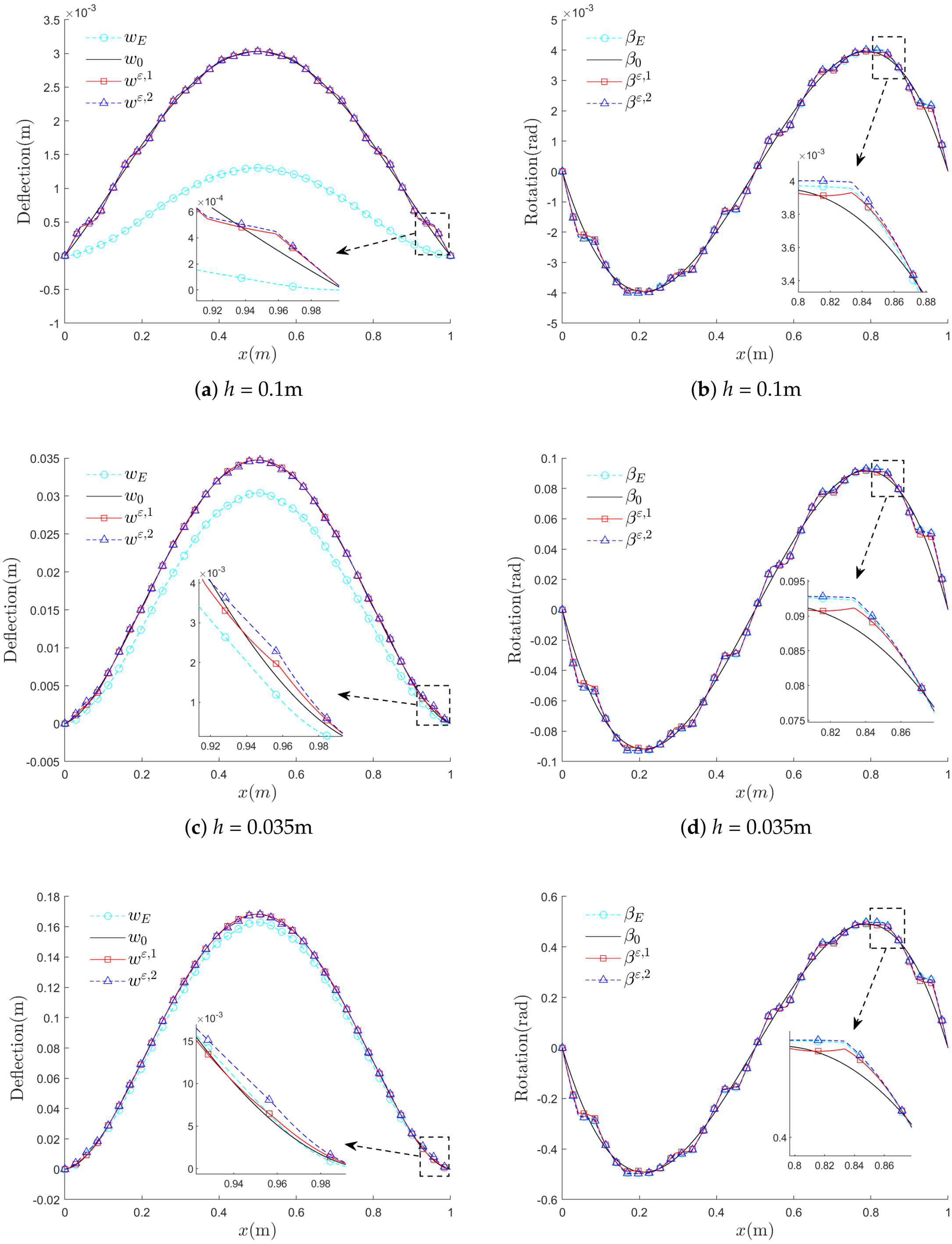

(**a**) h = 0.1m (**b**) h = 0.1m

(**c**) h = 0.035m (**d**) h = 0.035m

(**e**) h = 0.02m (**f**) h = 0.02m

Figure 14. Approximation of the deflection w_E and the rotation β_E by the SOTS computation ($\varepsilon = \frac{1}{8}$).

Table 8. Composite Timoshenko beam approaching the composite Euler beam ($h/L = 0.1$).

ε	$e^{\varepsilon,0}_{w,E}$	$e^{\varepsilon,1}_{w,E}$	$e^{\varepsilon,2}_{w,E}$	$e^{\varepsilon,0}_{\beta,E}$	$e^{\varepsilon,1}_{\beta,E}$	$e^{\varepsilon,2}_{\beta,E}$
$\frac{1}{4}$	1.3653	1.3700	1.3779	1.4292E-1	5.0342E-2	1.6830E-2
$\frac{1}{8}$	1.5184	1.5193	1.5211	6.9814E-2	1.2038E-2	8.7056E-3
$\frac{1}{16}$	1.5552	1.5555	1.5559	3.4706E-2	5.1497E-3	3.9123E-3
$\frac{1}{24}$	1.5449	1.5450	1.5452	2.2997E-2	3.9031E-3	2.5664E-3

doi:10.20944/preprints202510.0731.v1

Table 9. Composite Timoshenko beam approaching the composite Euler beam ($h/L = 0.035$).

ε	$e_{w,E}^{\varepsilon,0}$	$e_{w,E}^{\varepsilon,1}$	$e_{w,E}^{\varepsilon,2}$	$e_{\beta,E}^{\varepsilon,0}$	$e_{\beta,E}^{\varepsilon,1}$	$e_{\beta,E}^{\varepsilon,2}$
$\frac{1}{4}$	8.8101E-2	8.9562E-2	8.2858E-2	1.4672E-1	5.8046E-2	9.5688E-3
$\frac{1}{8}$	1.6484E-1	1.6498E-1	1.6314E-1	7.0325E-2	1.4389E-2	3.4649E-3
$\frac{1}{16}$	1.8606E-1	1.8609E-1	1.8563E-1	3.4635E-2	3.1767E-3	2.5024E-3
$\frac{1}{24}$	1.8617E-1	1.8618E-1	1.8599E-1	2.2993E-2	2.7956E-3	1.4163E-3

Table 10. Composite Timoshenko beam approaching the composite Euler beam ($h/L = 0.02$).

ε	$e_{w,E}^{\varepsilon,0}$	$e_{w,E}^{\varepsilon,1}$	$e_{w,E}^{\varepsilon,2}$	$e_{\beta,E}^{\varepsilon,0}$	$e_{\beta,E}^{\varepsilon,1}$	$e_{\beta,E}^{\varepsilon,2}$
$\frac{1}{4}$	3.9508E-2	4.0083E-2	4.2898E-2	1.4710E-1	5.8696E-2	9.3389E-3
$\frac{1}{8}$	3.8995E-2	3.9078E-2	3.6491E-2	7.0391E-2	1.4654E-2	3.1435E-3
$\frac{1}{16}$	5.7812E-2	5.7823E-2	5.7254E-2	3.4641E-2	3.2293E-3	2.3076E-3
$\frac{1}{24}$	5.8164E-2	5.8169E-2	5.7925E-2	2.2992E-2	2.7895E-3	1.4008E-3

6. Conclusions

A two-scale asymptotic framework is established for composite Mindlin plates and Timoshenko beams, demonstrating that the second-order correctors are crucial for accurately capturing stress oscillations at material interfaces. When h decreases, the asymptotic model developed can effectively approximate the Kirchhoff plate and Euler beam with composite configurations, respectively, providing an alternative way to simulate complicated thin plate and beam structures. The RIE and CIE are employed in the finite element computations of the homogenization models to mitigate shear locking, which can give an accurate description of the displacement and stress distributions of the plates and beams.

Most importantly, the proposed method offers significant potential for future work. It can be directly extended to model sustainable composites with valorised manufacturability. This establishes our asymptotic framework as a general and computationally efficient approach for predicting the multi-physical response of next-generation composite plates and beams, thereby contributing to the development of tailored material systems aligned with the goals of modern industrial applications.

Author Contributions: Conceptualization, M.Z., Q.M.; methodology, M.Z. and Q.M.; software, M.Z. and Q.T.; validation, M.Z., Q.M. and Q.T.; formal analysis, M.Z. and Q.M.; investigation, M.Z.; data curation, M.Z. and Q.T.; writing—original draft preparation, M.Z.; writing—review and editing, M.Z., Q.M.; visualization, M.Z.; supervision, Q.M. ; project administration, Q.T.; funding acquisition, Q.M. and Q.T. All authors have read and agreed to the published version of the manuscript.

Funding: This research was funded by the National Key R&D Program of China (No.2024YFA1012803), National Natural Science Foundation of China (U24B2073) and the Natural Science Foundation of Sichuan Province (Grant No.2024NSFSC0438).

Data Availability Statement: The data presented in this study are available on request from the corresponding author. The data are not publicly available due to privacy concerns.

Acknowledgments: The authors gratefully acknowledge the reviewers' constructive suggestions and insightful comments that have helped strengthen this research.

Conflicts of Interest: The authors declare no conflicts of interest.

References

1. Jangravi, S.; Masjedi, P.K.; Reali, A. Equilibrium-based 3D stress recovery of laminated anisotropic composite plates via isogeometric analysis. *Compos. Struct.* **2025**, *365*, 119144.
2. Patton, A.; Antolín, P.; Dufour, J.E.; Kiendl, J.; Reali, A. Accurate equilibrium-based interlaminar stress recovery for isogeometric laminated composite Kirchhoff plates. *Compos. Struct.* **2021**, *256*, 112976.

3. Wan, D.; Hu, D.; Natarajan, S. A linear smoothed quadratic finite element for the analysis of laminated composite Reissner-Mindlin plates. *Compos. Struct.* **2017**, 180, 395–411.
4. Lee, C.Y.; Yu, W.B. Homogenization and dimensional reduction of composite plates with in-plane heterogeneity. *Int. J. Solids Struct.* **2011**, 48(1), 1474–1484.
5. Huang, Z.W.; Xing, Y.F.; Gao, Y.H. A new method of stiffness prediction for composite plate structures with in-plane periodicity. *Compos. Struct.* **2021**, 280, 114850.
6. Cioranescu, D.; Donato, P. *An Introduction to Homogenization*; Oxford University Press: New York, USA, 1999.
7. Bensoussan, A.; Lions, J.L.; Papanicolaou, G. *Asymptotic Analysis for Periodic Structures*; North-Holland: Amsterdam, Netherlands, 1978.
8. Lions, J.L. *Some Methods in the Mathematical Analysis of Systems and Their Control*; Science Press, Gordon and Breach Science Publishers: Beijing, China, 1981.
9. Jikov, V.V.; Kozlov, S.M.; Oleinik, O.A. *Homogenization of Differential Operators and Integral Functional*; Springer-Verlag: Berlin-Heidelberg, Germany, 1994.
10. Hou, T.Y.; Wu, X.H. A multiscale finite element method for elliptic problems in composite materials and porous media. *J. Comput. Phys.* **1997**, 134, 169–189.
11. Abdulle, A.; E, W.N.; Engquist, B.; Vanden-Eijnden, E. The heterogeneous multiscale method. *Acta Numer.* **2012**, 21, 1–87.
12. E, W.N. *Principles of Multiscale Modeling*; Science Press: Beijing, China, 2012.
13. Cui, J.Z.; Cao, L.Q. Finite element method based on two-scale asymptotic analysis. *Math. Numer. Sin.* **1998**, 20(2), 89–102.
14. Cao, L.Q.; Cui, J.Z. Asymptotic expansions and numerical algorithms of eigenvalues and eigenfunctions of the Dirichlet problems for second order elliptic equations in perforated domains. *Numer. Math.* **2004**, 96, 528–581.
15. Cao, L.Q.; Cui, J.Z.; Zhu, D.C. Multiscale asymptotic analysis and numerical simulation for the second order Helmholtz equations with rapidly oscillating coefficients over general domains. *SIAM J. Numer. Anal.* **2002**, 40(2), 543–577.
16. Ma, Q.; Cui, J.Z.; Li, Z.H.; Wang, Z.Q. Second-order asymptotic algorithm for heat conduction problems of periodic composite materials in curvilinear coordinates. *J. Comput. Appl. Math.* **2016**, 306, 87–115.
17. Ma, Q.; Cui, J.Z. Second-order two-scale analysis method for the quasi-periodic structure of composite materials under condition of coupled thermo-elasticity. *Adv. Mater. Res.* **2013**, 629, 160–164.
18. Dong, H.; Zheng, X.J.; Cui, J.Z.; Nie, Y.F.; Yang, Z.Q.; Yang, Z.H. High-order three-scale computational method for dynamic thermo-mechanical problems of composite structures with multiple spatial scales. *Int. J. Solids Struct.* **2019**, 169(1), 95–121.
19. Yang, Z.H.; Cui, J.Z.; Wu, Y.T.; Wang, J.Q.; Wan, J.J. Second-order two-scale analysis method for dynamic thermo-mechanical problems in periodic structure. *Int. J. Numer. Anal. Model.* **2015**, 12(1), 144–161.
20. Feng, Y.P.; Cui, J.Z. Multi-scale analysis and FE computation for the structure of composite materials with small periodicity configuration under condition of coupled thermo-elasticity. *Int. J. Numer. Methods Eng.* **2004**, 60, 241–269.
21. Su, F.; Cui, J.Z.; Xu, Z.; Dong, Q.L. Multi-scale method for the quasi-periodic structures of composite materials. *Appl. Math. Comput.* **2011**, 217, 5847–5852.
22. Caillerie, D. Thin elastic and periodic plates. *Math. Methods Appl. Sci.* **1984**, 6, 159–191.
23. Lewiński, T.; Józef, J.T. *Plates, Laminates, and Shells: Asymptotic Analysis and Homogenization*; World Scientific: River Edge, NJ, USA, 2000.
24. Zhu, G.Q.; Cui, J.Z. Second-order two-scale method for bending behaviors of composite plate with periodic configuration. *AIP Conf. Proc.* **2010**, 1233(1), 1088–1093.
25. Wang, Z.Q.; Cui, J.Z. Second-order two-scale method for bending behavior analysis of composite plate with 3-D periodic configuration and its approximation. *Sci. China Math.* **2014**, 57, 1713–1732.
26. Huang, Z.W.; Xing, Y.F.; Gao, Y.H. Two-scale asymptotic homogenization method for composite Kirchhoff plates with in-plane periodicity. *Aerosp.* **2022**, 9(12), 751.
27. Huang, Z.W.; Xing, Y.F.; Gao, Y.H. A two-scale asymptotic expansion method for periodic composite Euler beams. *Compos. Struct.* **2020**, 241, 112033.
28. Aguirre, A.; Codina, R.; Baiges, J. A variational multiscale stabilized finite element formulation for Reissner-Mindlin plates and Timoshenko beams. *Finite Elem. Anal. Des.* **2023**, 217, 103908.
29. Lepe, F.; Mora, D.; Rodríguez, R. Locking-free finite element method for a bending moment formulation of Timoshenko beams. *Comput. Math. Appl.* **2014**, 68(3), 118–131.

doi:10.20944/preprints202510.0731.v1

30. Falk, R.; Tu, T. Locking-free finite elements for the Reissner-Mindlin plate. *Math. Comp.* **2000**, 69(231), 911–928.